Asociación Argentina
de Mecánica Computacional

Mecánica Computacional Vol XXXIII, págs. 3503-3514 (artículo completo)
Graciela Bertolino, Mariano Cantero, Mario Storti y Federico Teruel (Eds.)
San Carlos de Bariloche, 23-26 Setiembre 2014

DIRECT NUMERICAL SIMULATION OF COMBINED TURBULENT CHANNEL FLOW

Vicente G. Gil Montero[a], Mariano I. Cantero[a] and Francisco Pedocchi[b]

[a]*Departamento de Mecánica Computacional, Centro Atómico Bariloche, Argentina*
gastongilmontero@gmail.com

[b]*Universidad de la República, Uruguay*

Keywords: turbulent channel oscillatory flow, combined flow, direct numerical simulation

Abstract. Wave-current processes are often observed in many different physical problems such as the flow in estuaries, beaches, etc. In these cases the pure current flow is modified due to the presence of waves. The propagation of waves can increase or decrease the streamwise current intensity depending on the direction of waves as it has been observed in laboratory experiments. The purpose of this work is to analyze the nonlinear effects of wave amplitude and wave period on turbulence characteristics of combined flow by means of Direct Numerical Simulation of the 3-D Navier-Stokes Equation. The effect of a wide range of frequencies and amplitude of the driving pressure gradient is reported and discussed.

1 INTRODUCTION

Waves are usually superimposed on currents in coastal regions. This interaction which mostly is non-linear, takes place mainly in estuaries and beaches and plays an important role in the local hydrodynamics and sediment transport processes. Therefore wave-current interaction has been the subject of many studies in the last decades. Among the studies based in laboratory measurements can be mentioned Kemp and Simons (1981), Lodahl et al. (1998), Umeyama (2009) and Musumeci et al. (2006) which observed that when waves and current interact the mean velocity profile and the turbulent properties of the current are significantly changed. The mean velocities near a smooth bed are increased by the presence of waves, while in rough bed they are reduced. Moreover, the results suggest that wave current interaction effects are not restricted to the near bed region, since they may propagate in the entire water column.

Numerical simulation studies as Scotti and Piomelli (2001) and Olabarrieta et al. (2010) have analysed combined flows and their models were able to reproduce the experimental observations carried out by the aforementioned investigators. There exist a wide range of flow conditions to be studied and, in spite of the fact that many researches have began to lighten the wave-current interaction, still litle is known about the complex mechanics that takes place in the cross angle case.

The present study is focused on the numerical simulation by DNS of an oscillatory motion orthogonal to a current. The main advantage of using DNS is that the whole range of spatial and temporal scales of the turbulence are simulated. Consequently all the spatial scales of the turbulence are resolved, from the smallest dissipative scales (Kolmogorov microscales) up to the channel height (associated with the motions containing most of the kinetic energy).

As a first step in the study of orthogonal combined flow the main objective of the present investigation is to study the case when the current velocity and the oscillating maximum velocity are of the same order of magnitude. The paper is organized as follows: in section 2 we present the problem formulation with the numerical model description and implementation. In section 3 we specify the studied cases parameters meanwhile in section 4 we expose the main results obtained by DNS. Finally in section 5 we summarize our conlusions after analysing the results.

2 PROBLEM FORMULATION

This work considers the flow in a horizontal channel driven by a mean pressure gradient in a direction tangential to the wall. The coordinate system is represented by the coordinates x, y, and z associated to unit vectors $\mathbf{i}$, $\mathbf{j}$, and $\mathbf{k}$ in the streamwise, spanwise, and vertical directions, respectively. The velocity field is represented by $\mathbf{u} = u\mathbf{i} + v\mathbf{j} + w\mathbf{k}$. The mean pressure gradient is given by

$$\frac{\partial p}{\partial x} = -\frac{G_u}{\rho} \tag{1}$$

$$\frac{\partial p}{\partial y} = -\frac{G_\omega}{\rho}\left[cos(\omega t)\right] \tag{2}$$

where ρ is the fluid density, ω is the oscillating frequency, G_u is the uniform pressure gradient, and G_ω is the amplitude of the oscillating pressure gradient.

The dimensionless form of the Navier–Stokes equations are obtained using the shear velocity $u_* = \sqrt{G_u H/\rho}$ as velocity scale, the channel height $L = H$ as length scale, $T = \sqrt{\rho H/G_u}$ as time scale and $P = G_u H$ as pressure scale . With these scales the dimensionless form of the

governing equations become

$$\frac{D\tilde{\mathbf{u}}}{D\tilde{t}} = -\tilde{\nabla}\tilde{p} + \frac{1}{R_{e*}}\tilde{\nabla}^2\tilde{\mathbf{u}} + \alpha cos(\tilde{\omega}\tilde{t})\mathbf{j} + \mathbf{i} \tag{3}$$

where $\alpha = \frac{G_\omega}{G_u}$, $R_{e*} = \frac{H\sqrt{\frac{G_u H}{\rho}}}{\nu}$ and $\tilde{\omega} = \omega\sqrt{\frac{\rho H}{G_u}}$,

The Navier Stokes equations were solved using a de-aliased pseudospectral code (Canuto et al., 1988). Fourier expansions were employed for the flow variables in the horizontal directions (x and y are the streamwise and spanwise directions, respectively). In the inhomogeneous vertical direction (z) a Chebyshev expansion was used with Gauss-Lobatto quadrature points. An operator splitting method was used to solve the momentum equation along with the incompressibility condition (see Brown et al. (2001)). First, an advection-diffusion equation was solved to compute an intermediate velocity field. After this intermediate velocity field was computed, a Poisson equation was solved to compute the pressure field. Finally, a pressure correction step was performed to obtain the final incompressible velocity field. A low-storage mixed third order Runge-Kutta and Crank-Nicolson scheme was used for the temporal discretization of the advection-diffusion terms. More details of the implementation of this numerical scheme can be found by Cortese and Balachandar (1995). Validation of the code can be found by Cantero et al. (2007a), Cantero et al. (2007b) and Pedocchi et al. (2010).

The dimensions of the computational domain are L_x=$2\pi H$, L_y=$2/3\pi H$, and L_z=$2H$. The grid resolution used is $N_x = 128 \times N_y = 128 \times N_z = 192$ and the nonlinear terms were computed in a grid $3N_x/2 \times 3N_y/2 \times N_z$ in order to prevent aliasing errors. The top wall and the bottom wall represent a smooth no-slip boundary to the flow.

Periodic boundary conditions have been implemented in the two horizontal directions (implying homogeneous flow in the streamwise and spanwise directions).This can be done since the computation domain has been chosen to include the largest eddies in the flow and therefore the domain is large enough to prevent correlative fluctuations.

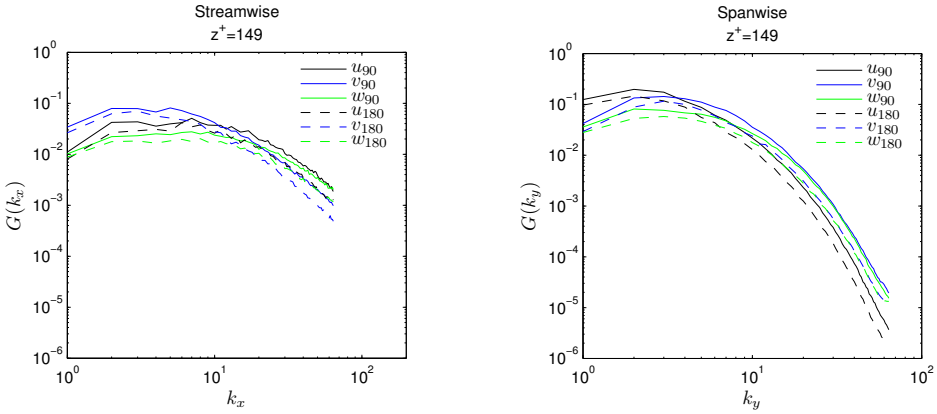

Figure 1: F3 horizontal spectra. The phase ph=90 corresponds to the maximum oscillating velocity, meanwhile ph=180 corresponds to the maximum pressure gradient

Fig. 1 shows the one dimensional spectra corresponding to the most demanding case of study. This figure shows the phases of maximum spanwise velocity (at phase 90°) and maximum pressure gradient (at phase 180°) corresponding to the horizontal directions. The energy spectra show that the grid resolution is adequate, since the energy asociated with the high wavenumber is at least two times lower than the energy density corresponding to low wave numbers for the

cases of the most demanding flow phases (Kim et al., 1986). Finally it can be observed that there is non energy pile-up at high wavenumbers.

In unsteady flows special averaging operators need to be defined in order to study the flow paterns. First a quantity can be averaged over planes of homogeneity (x and y planes) and time,

$$U(z) = \frac{1}{NL}\sum_{l=1}^{L}\sum_{n=1}^{N}\frac{1}{RM}\sum_{r=1}^{R}\sum_{m=1}^{M} u(r\Delta x, m\Delta y, z, l(n-1)) \tag{4}$$

where N is the number of cycles to average, L is the number of phases by cycle, $R = L_x/\Delta x$ is the number of points in the x direction and $M = L_y/\Delta y$ is the number of points in the y direction. Beside the plane and time averaging, phase averaging is meaningful to study periodic systems as the present one. Hence we have phase averaged quantities defined as follow;

$$\overline{u}(z,t) = \frac{1}{N}\sum_{n=1}^{N}\frac{1}{RM}\sum_{r=1}^{R}\sum_{m=1}^{M} u(r\Delta x, m\Delta y, z, t + L(n-1)) \tag{5}$$

The three studied flow cases (see Table 1) where initialized from the DNS results of a current channel flow. In order to reach a statistically steady state 10 cycles were simulated. In all the cases the time evolution of the friction velocity and mean velocities were monitored until a steady state was reached. After, 20 complete cycles were simulated in order to obtained the convergence of first and second order statistics.

3 CASES OF STUDY

In order to study the orthogonal flow, we fixed the ratio U_u/U_ω and explore the effect of different oscillating regimes on the current flow. The regime flow is described by three parameters: 1) the mean flow characterized by the Reynolds number R_{e*}, 2) the forcing frequency $\tilde{\omega}$ and 3) the ratio between the uniform pressure gradient and the amplitude of the oscillating pressure gradient α. In all of our numerical experiments we have kept $R_{e*} = u * H/\nu$=180 constant and we have changed $\tilde{\omega}$ and α in order to observe the wave effect on the current flow. In Table 1 the flow simulated parameters are detailed.

Flow	R_{e*}	α	$\tilde{\omega}$	Frequency
F1	180	500	25	High
F2	180	100	5	Intermediate
F3	180	10	0.5	Low
F4	180	-	-	-

Table 1: Parameters used for the simulations.

The thickness of the viscous oscillating layer in viscous units is

$$\delta^+ = \sqrt{\frac{2\nu}{\omega}}\frac{u_*}{\nu} \tag{6}$$

And the oscillating Reynolds number is defined as

$$R_\omega = \frac{AU_0}{\nu} \tag{7}$$

where A is the maximum wave intrution and U_0 is the maximum orbital velocity

Flow	u_{*max}	δ^+	$\frac{U_u}{U_\omega}$	R_ω	Φ
F1	0.97	3.7	1.05	3292	45
F2	1.01	8.6	0.97	15729	43
F3	1.11	29.9	0.75	179624	16

Table 2: Mean flow variables.

Table 2 shows the parameters that characterize the flow. In Table 2 Φ is the phase lead of the maximum bed shear stress over the maximum free-stream velocity. In the case of F1, which corresponds to a laminar oscillating regime, the height of the viscous layer remains in the viscous layer (y^+=5). In F2, which correspons to a disturbed laminar regime, the viscous oscillating layer is confined in the range $5 < y^+ < 30$ and it has reaches the buffer layer of the current flow. In the last case, F3, the height of the oscillating viscous layer is equal to 29.8 and can be said that it almost reaches the logarithmic layer of the current flow (y^+>30).

4 RESULTS AND DISCUSSION

4.1 Mean velocities

Figure 2 shows profiles of the mean dimensionless streamwise velocity ($U/U*$) as function of the dimensionless distances from the wall $zu*/\nu$. Here the mean shear velocity U_* corresponds to the average of the shear velocities by phase. It is observed that when a current is superimposed to an orthogonal oscillation the velocity profile of the current undergoes transformations due to the orthogonal oscillatory flow. Depending on the frequency of the oscillation the friction factor can give a rise or decrease. In the particular cases of F1 and F2 the mean streamwise velocity is increased independently of the phase cycle. On the other hand in F3, the entire column water is affected by the oscillation. Moreover the motion in the current direction has both a steady component and an oscillatory one, as a consequence of the wave added to the current. This wave effect on the current was also observed in experimental measurement carried out by Musumeci et al. (2006).

In order to study the effect of the orthogonal oscillating flow on the current flow the Von Karman (k) and B constants from the logarithmic law, were calculated from DNS results of the mean streamwise velocity by minimum square method. In Table 3 are detailed the logaritmic law parameters obtained.

$$\frac{U}{U*} = \frac{1}{k} ln \left(\frac{z u_{*max}}{\nu} \right) + B \tag{8}$$

The Von Karman constant relates the $U(z)$ profiles along z in a wall bounded shear flow to the shear stress at the bed surface, therefore it is related to the friction factor. Meanwhile the parameter B shifts upwards or downwards the curve according to the modulation of the free stream velocity. The Von Karman constants obtained for the studied flows remain below the corresponding value for a channel flow. A Von Karman constant reduction was reported in flows with bed load transport, in which k can be reduced to almost 0.29 (Nicora and Goring, 2000). This reduction in k probably indicates that the F1 and F2 may belong to a wide class of drag reducing flows. This suggestion finds support in the decreased friction factor, which is going to be further discussed in section 4.4. The exact mechanisms for drag reduction are still unclear, but many researchers attribute it to modifications of bursting events or largescale coherent structures. In many cases it has been observed that k reduces when spanwise spacing between structures increases whereas streamwise spacing does not change (Nicora and Goring,

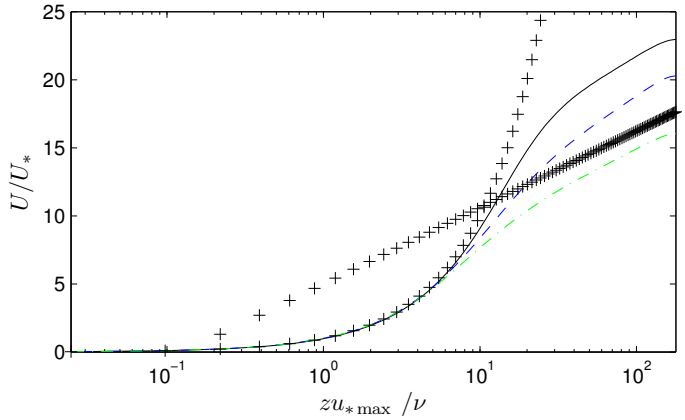

Figure 2: Streamwise mean velocity (U/U_*). The solid line (–) corresponds to F1, the dashed line (- -) to F2, the dotted dashed line (- ·) to F3 and the cross mark line (+) correponds to the log. Law and wall Law.

2000).

Flow	k	B	U_*
F1	0.33	7.6	0.973
F2	0.30	3.3	1.001
F3	0.40	3.6	0.995

Table 3: Logarithmic law parameters.

Vertical profiles of spanwise velocity ($\overline{v}/u_{*max}$) at different phases are shown in Figure 3. During the accelation stage, the velocity increases rapidly in the three cases throughout the boundary layer and the maximum velocity moves upwards. This maximum velocity is presented as an overshoot for F1 but as the oscillating frequency decreases, F2 and F3, it tends to disappear. Stronger coupling between the inner and the outer layers occurs as the oscillating frequency is reduced. This behavior goes on during the deceleration stage with the adverse pressure gradient that reduces progressively the velocity. Therefore the boundary layer grows even after eventually the reverse near-wall flow commences and the entire flow turns back forming in the opposite direction a new boundary layer. A phase with zero wall shear stress occurs at 134°, 136° and 157° for F1, F2 and F3 respectively.

In Figure 4 are shown the free streamwise ($\overline{u}/u*$) and spanwise ($\overline{v}/u*$) velocities by phase. A sinusoidal behavior of the free streamwise velocity is observed only in F3, probably due to the fact that the oscillating thickness layer reached the core of the channel. Beside it can be noticed that the two free streamwise velocity maximum are in phase with the two free spanwise velocity maximum and the streamwise velocity minimum is coincident with the zero spanwise velocity. In subfigure (b) it can be noted that in F3 the free spanwise velocity does not behave as a perfect sine, since it is slightly far along. Meanwhile in F1 and F2 present a sine form.

4.2 Stress tensor

Vertical distributions of the the $\overline{u'w'}/u^2_{*max}$ mean shear stress component of the simulated cases are shown in Figure 5. In the laminar regime of R_ω, F1, the $\overline{u'w'}/u^2_{*max}$ mean shear stress component presents a reduction of its magnitude. This indicate that the turbulence in the streamwise direction is not completely developed. On the contrary in the disturbed laminar and intermitent turbulent cases F2 and F3 respectively, the mean shear stress oscillates around the

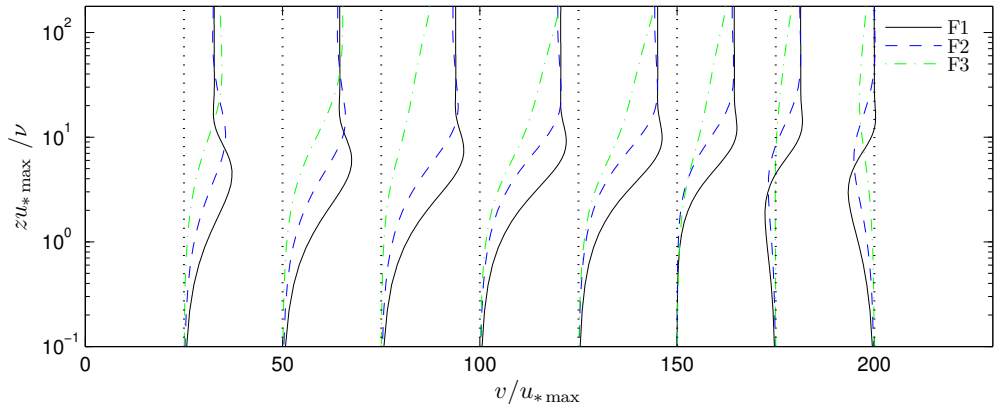

Figure 3: Spanwise mean velocity by phase (V/u_{*max}). The phases increase by 23° from left (22°) to right (180°)

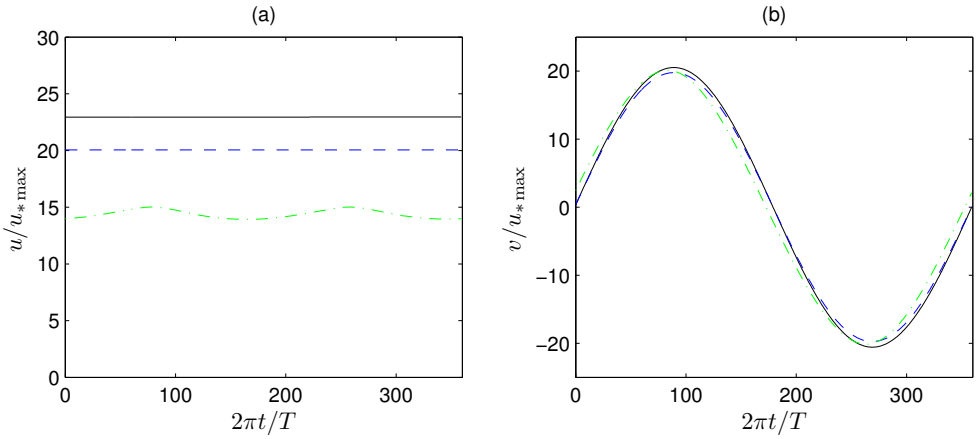

Figure 4: Mean free streamwise (a) and spanwise (b) dimensionless velocity by pase at z^+=180. The solid line (–) corresponds to F1, the dashed line (- -) to F2 and the dotted dashed line (- ·) to F3.

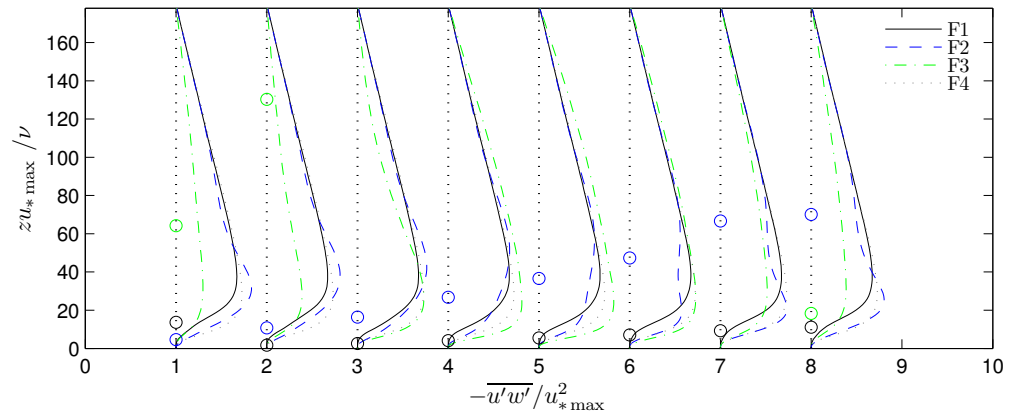

Figure 5: Phase averaged Reynolds Shear Stress ($\overline{u'w'}/u^2_{*max}$). Profiles are $T/16$ apart and are offset by 1 units in the horizontal direction starting from phase 22°. The circles indicate the respectively locations of the first zero crossing of the shear stress $\overline{v'w'}$ component, which is closed to the spanwise velocity maximum.

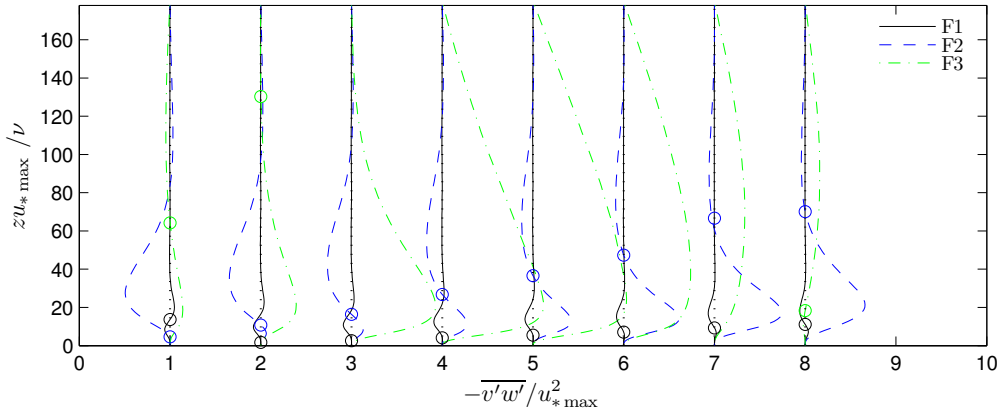

Figure 6: Phase averaged Reynolds Shear Stress ($\overline{v'w'}/u^2_{*max}$). Profiles are $T/16$ apart and are offset by 1 units in the horizontal direction starting from phase 22°. The circles indicate the respectively locations of the first zero crossing of the shear stress $\overline{v'w'}$ component, which is closer to the spanwise velocity maximum.

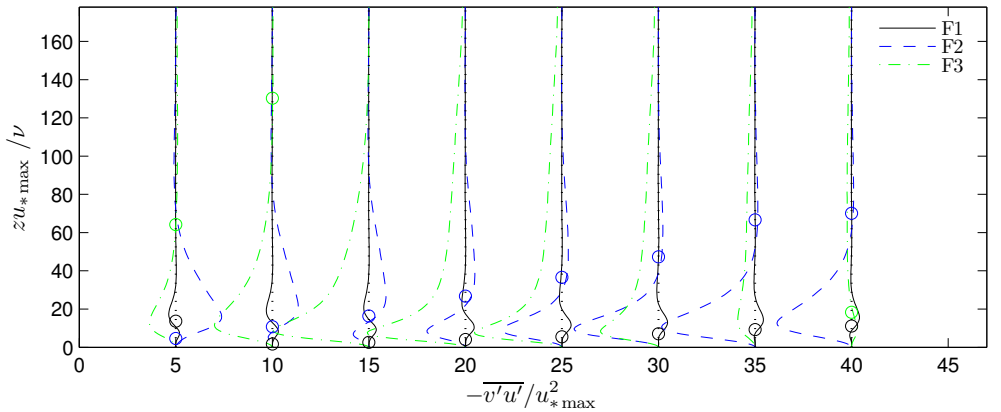

Figure 7: Phase averaged Reynolds Shear Stress ($\overline{u'v'}/u^2_{*max}$). Profiles are $T/16$ apart and are offset by 5 units in the horizontal direction starting from phase 22°. The circles indicate the respectively locations of the first zero crossing of the shear stress $\overline{v'w'}$ component, which is closer to the spanwise velocity maximum.

pure current case values. In the colineal combined flow experiments developed by Lodahl et al. (1998) it was noticed the same behavior.

Figure 6 are plotted vertical profiles of the Reynolds shear stress $\overline{v'w'}/u^2_{*max}$ at various phases during half of the cycle. In the low frequency regime the maximum takes places at phase 90° but meanwhile the oscillating frequency is enlarged, for example for case F3 this is delayed until the phase 157° and its magnitude becomes smaller, but in all the cases it occurs close to the wall. In the outer layer, $\overline{v'w'}/u^2_{*max}$ decreases more rapidly with the oscillating frequency. During the decelaration stage there is an increasing amount of $\overline{v'w'}/u^2_{*max}$ away from the wall owing to large scale turbulent structures that have a larger development when the oscillating flow approach to a stationary state.

The location of the first zero shear stress tensor value of $\overline{v'w'}/u^2_{*max}$ component is defined as the boundary layer thickness, which it is assumed to be coincident with the location where the maximum velocity takes place. This definition was first adopted by Sumer, Jensen and Fredsøe. As was observed by Pedocchi et al. (2010) in a pure oscillating transitional turbulent flow, the location of the zero Reynolds shear stress $\overline{v'w'}/u^2_{*max}$ never exatly coincides with the location of the oscillating maximum velocity. Nevertheless this assumption is in good agreement with the steady boundary layer definition. It is observed that the maximum boundary layer is the upper limit of the oscillating effect on the flow. Above it, prevails the current alone flow properties. Therefore only in F3 the oscillating effects are felt in the entire column water, due to the boundary layer reaches the core of the simulated channel.

Figure 7 shows vertical profiles of the Reynolds shear stress $\overline{u'v'}/u^2_{*max}$ by phase. It is remarkable the coupling between the zero value of $\overline{u'v'}/u^2_{*max}$ with those of $\overline{v'w'}/u^2_{*max}$.

4.3 Shear velocity

Figure 8 shows the streamwise and spanwise shear stress velocities by phase. The solid line corresponds to the spanwise shear velocity meanwhile the dashed line corresponds to the streamwise velocity. It can be pointed out how the mean shear stresses velocity profiles deform as R_ω rises. In the case of F3, subfigure (c), it can be observed a second maximum in the stage of the flow deceleration. This was also noted by Jensen (1988) but at a higher oscillating Reynolds number (R_ω=2.9x10^5).

The streamwise shear velocity behavior is also interesting. As far as the oscillating layer thickness reaches the core of the channel, a sinusoidal behavior appears and grows with the Reynolds. This indicates that there is a strong coupling between the pure current channel flow and the oscillating flow.

4.4 Friction factor and phase lag

The friction factor and the phase lag are important tools to predict whether the flow regime will be laminar, transitional or turbulent. Since the hydrodynamics state of the studied flows is the result of a current superimposed with an orthogonal wave, therefore a current friction factor (F_c) and a wave friction factor (F_ω) can be defined according to the flow direction,

$$F_c = \frac{T_x}{\rho U^2} \tag{9}$$

$$F_\omega = \frac{2\overline{\tau_{ym}}}{\rho \overline{v_m^2}} \tag{10}$$

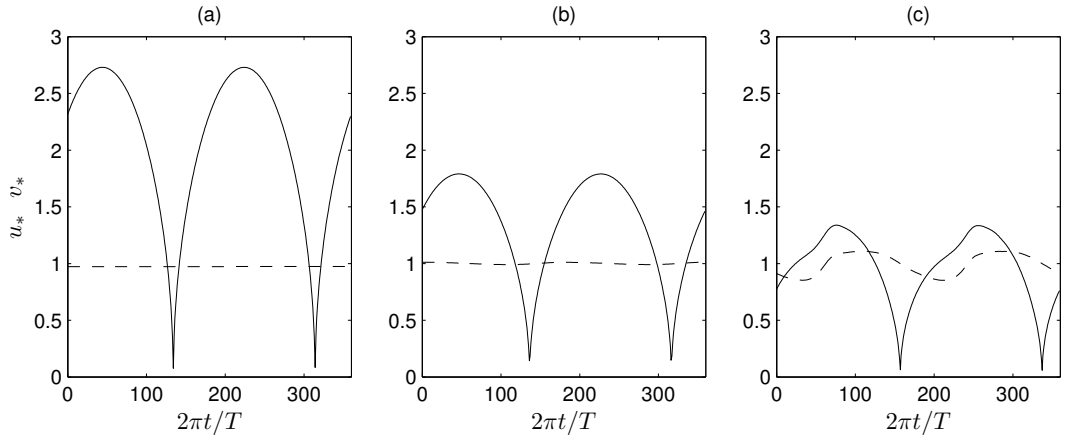

Figure 8: Streamwise (u_*) and spanwise (v_*) shear stress velocity by phase. The continue line (–) corresponds to v_* and the dashed line (- -) to u_*. The subfigure (a), (b) and (c) correspond to F1, F2 and F3 respectively.

where T_x is mean streamwise bed shear stress, U is the mean streamwise velocity, $\overline{\tau_{ym}}$ is the maximum spanwise bed shear stress and $\overline{v_m}$ is the maximum spanwise velocity. Table 4 presents the corresponding friction factors for the studied flows.

In the oscillating laminar regime, the laminar wave friction factor ($F_{\omega l}$) depending on the Reynolds number is defined as,

$$F_{\omega l} = \frac{2}{\sqrt{R_\omega}} \tag{11}$$

Flow	F_c	F_ω	$F_{\omega l}$
F1	0.0026	0.0326	0.0348
F2	0.0035	0.0147	0.0159
F3	0.0054	0.0072	0.0047
F4	0.0046	-	-

Table 4: Friction factor coefficients associatted to the simulated flows.

In the case of the current friction factor it can be observed from Table 4 that the two first reported flows present a smaller friction factor than the alone current case (F4), but the third flow presents a bigger current friction factor. Therefore meanwhile the oscillating flow remains in the laminar regime according to its oscillating Reynolds number, there is a reduction of the current friction factor. On the other hand the wave friction factor of the two low oscillating Reynolds flows remains almost without change in comparison with the pure oscillating flow case. Nevertheless the highest oscillating Reynolds number simulated flow presents an increasing value of the current friction factor and wave friction factor in comparison with the respectively pure cases.

The phase lag in the spanwise direction between the free velocity and the shear stress velocity is also a helpful parameter to characterize the flow regime. In the laminar regime the phase lag is 45°, but as the turbulence develops this lag tends to diminish. In Table 1 are shown the phase lag in degrees. According to the reported data from DNS only the first flow is considered to be laminar because its phase lag value is 45°, meanwhile the others two fall in the transitional stage according to the phased lead diagramm proposed by Jensen (1988). The DNS results suggest that the transional turbulence stage of the combined flow comes early in comparison with the pure oscillating case.

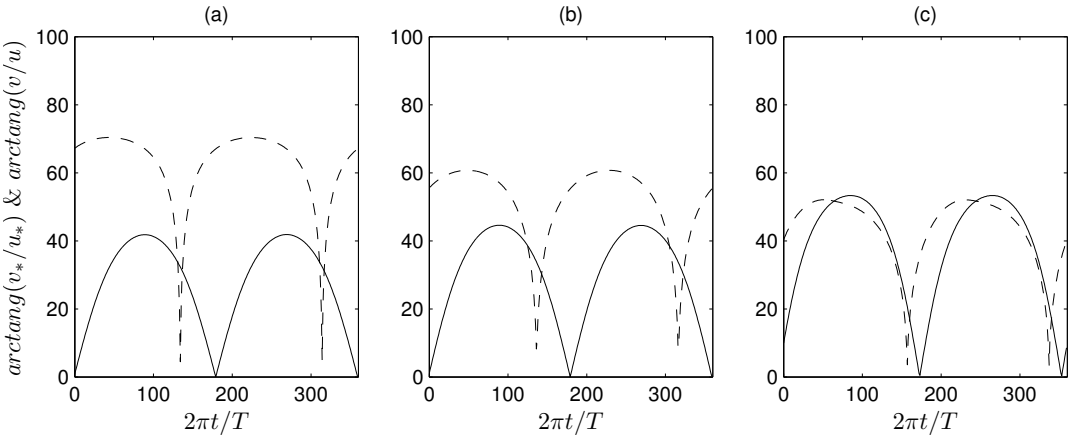

Figure 9: Angle of the free velocity and shear velocity. The solid line (-) corresponds to free velocity direction meanwhile the dashed line (- -) corresponds to the wave shear velocity direction. The subfigure (a), (b) and (c) correspond to F1, F2 and F3 respectively.

Also another phase lag can be defined, because of the lack of collinearity between the wave and the current, as the difference between the shear stress direction and the free velocity direction. In Figure 9 can be noticed the phase lag between the oscillating free-stream velocity and the shear-stress velocity. This phase lag agrees with the phase lag between the free velocity and the shear stress velocity. An interesting fact is that the maximum change direction angle of the freem velocity grows meanwhile the maximum friction velocity angle decreases when the oscillating Reynolds number grows. This is expected since the turbulence has time to diffuse vertically as the oscillating frequency decreases with higher oscillating Reynolds numbers.

5 CONCLUSIONS

The combined flow generated by the interaction at a right angle of a current with waves is numerically investigated. The effect of the oscillatorry flow on the current is analysed by performing simulations from the laminar oscillating regime up to the turbulent oscillating intermittent regime. In order to study this interaction the current Reynolds number is fixed, meanwhile α and ω are modified in such a way to keep approximately constant the relation u_c/u_ω but changing the flow regime.

When an oscillatory flow is superimposed on a turbulent current, the friction factor can rise or decrease depending on the oscillating frequency. According to the studied cases, if the dimensional oscillating frequency remains above 5, the friction factor is reduced in comparison with the pure current case otherwise the contrary was reported.

The oscillating flow effect on the current depends on the thickness of the oscillating boundary layer. It was observed that the oscillating boundary layer thickness grows and eventually vanishes depending on the cycle stage. Above the maximum oscillating boundary layer thickness the oscillating characteristics are negligible, but if it reaches the core channel the oscillation affects the entire column water and a strong coupling between the streamwise and spanwise direction appears.

The obtained results also show that the Von Karman constant, which indicates the relation between the $U(z)$ profiles along z and the bed shear stress, for the mean streamwise velocity addopts values smaller than 0.42, indicating that the orthogonal oscillating flow may belong to a wide class of drag-reducing flows.

Regarding the effect of the current on the oscillating flow it can be concluded that the turbulence is increased by the presence of the current in the orthogonal direction. This is observed

since the phase lag and the wave friction factor of the simulated cases correspond to flow with higher oscillating Reynolds number reported by numerical and experimental investigations.

REFERENCES

Brown D., Cortez R., and M.L. M. Accurate projection methods for the incompressible navier-stokes equations. *Journal of Computational Physics*, 168:464–499, 2001.

Cantero M., Balachandar S., and Garcia M. High-resolution simulations of cylindrical density currents. *Journal of Fluid Mechanics*, 590:437–469, 2007a.

Cantero M., Balachandar S., and Garcia M. On the front velocity of gravity currents. *Journal of Fluid Mechanics*, 586:1–39, 2007b.

Canuto C., Husssaini M., Quarteroni A., and Zang T. *Spectral Methods in Fluid Dynamics*, volume I. Springer-Verlag, 1988.

Cortese T. and Balachandar S. High perfomance spectral simulations of turbulent flows in massively parallel machines with distributed memory. *International Journal of High Performance Computing Applications*, 9:187–204, 1995.

Jensen B. *Experimental investigation of turbulent oscillatory boundary layer*, volume I. Series Paper 45, Technical University of Denmark, 1988.

Kemp P. and Simons R. The interaction between waves and a turbulent current: waves propagationg with the current. *Journal of Fluid Mechanics*, 116:227–250, 1981.

Kim J., Moin P., and R. M. Turbulence statistics in fully developed channel flow at low reynolds number. *Journal of Fluid Mechanics*, 177:133–166, 1986.

Lodahl C., Sumer B., and Fredsoe J. Turbulent combined oscillatory flow and current in a pipe. *Journal of Fluid Mechanics*, 373:313–348, 1998.

Musumeci R., Cavallaro L., Foti E., Scandura P., and Blondeaux P. Waves plus currents crossing at right angle. 111:C07019, 2006.

Nicora V. and Goring D. Flow turbulence over fixed and weakly mobile gravel beds. *Journal of Hydraulic Engineering*, 127:123–133, 2000.

Olabarrieta M., Medina R., and Castanedo S. Effect of wave current interaction on the current profile. *Journal of Coastal Engineering*, 57:643–655, 2010.

Pedocchi F., Cantero M., and M. G. Turbulent kinetic energy balance of an oscillatory boundary layer in the transition to the fully turbulent regime. *Journal of Turbulence*, 12:1–27, 2010.

Scotti A. and Piomelli U. Numerical simulation of pulsating turbulent channel flow. *Physics of Fluids*, 13:1367–1384, 2001.

Umeyama M. Changes in turbulent flow structure under combined wave-current motions. *Journal of Waterway, Port, Coastal and Ocean Engineering*, 5:213–227, 2009.